Soft Matter

PAPER

View Article Online
View Journal | View Issue

Cite this: *Soft Matter*, 2025, **21**, 5998

Optimal first-passage times of active Brownian particles under stochastic resetting

Yanis Baouche [a] and Christina Kurzthaler *[abc]

We study the first-passage-time (FPT) properties of an active Brownian particle under stochastic resetting to its initial configuration, comprising its position and orientation, to reach an absorbing wall in two dimensions. We employ a renewal framework for the stochastic resetting process and use a perturbative approach for small Péclet numbers, measuring the relative importance of self-propulsion with respect to diffusion. This allows us to derive analytical expressions for the survival probability, the FPT probability density, and the associated low-order moments. Depending on their initial orientation, the minimal mean FPT for active particles to reach the boundary can both decrease and increase relative to the passive counterpart. The associated optimal resetting rates depend non-trivially on the initial distance to the boundary due to the intricate interplay of resetting, rotational Brownian noise, and active motion.

Received 3rd April 2025,
Accepted 16th June 2025

DOI: 10.1039/d5sm00340g

rsc.li/soft-matter-journal

I. Introduction

Stochastic resetting is a relatively recent concept whereby a process is randomly reset to a predetermined state. Mainly introduced in the context of search processes with Brownian motion,[1,2] this framework has been widely expanded to take into account other types of processes, such as Lévy flights,[3–5] non-Poissonian waiting times,[6–9] or partial,[10,11] time-dependent,[12] or random resetting mechanisms.[13] Overall, stochastic resetting has proven to be a very fruitful research direction for the physics community with a variety of applications. The most common applications being algorithmics,[14–17] chemical reactions,[18–20] and animal foraging.[21,22] In all of those applications, resetting prevents being trapped in a suboptimal state (*e.g.*, resource- or reactant-depleted zone), and most importantly, expedites the search completion (food sources, reactants, or optima), thus improving performance when time constraints are imposed.

The question of FPT properties is particularly important in the context of biology, where the efficiency during foraging is a crucial part of a microorganism's ability to survive and achieve its biological purpose.[23–29] Using biology as a model system, active agents have been engineered in the lab and extract energy from their environment to self-propel.[30–34] Establishing a physical understanding of how fast these active colloids reach specific targets is an important aspect in their design for target-delivery and bioremediation applications.[35–37] Because of the coupling between translational and rotational degrees of freedom, studying the FPT properties of active agents is arguably more difficult than the passive (Brownian) counterpart, but can also lead to a richer variety of results.[38–44] In this paper, we study one of the paradigmatic models of active matter – the active Brownian particle (ABP) – comprising the effect of active motion, translational and rotational diffusion.[45–49]

It is well-established that resetting a passive tracer to its original position enables a stationary distribution and a finite mean FPT (MFPT) for reaching the target.[1,50,51] Yet, the interplay of resetting with active motion has not yet been studied in the context of FPT statistics. In our recent work,[52] relying on a perturbation analysis for low Péclet numbers, we find that the typical Brownian scaling of the survival probability $S(t) \propto t^{-1/2}$ is preserved, yet with a distinct prefactor depending on the agent's initial orientation. Even though the MFPT remains undefined, the median proves to be a robust metric, able to capture the new dynamics emerging from the rotational degree of freedom. Building upon our recent findings for the ABP and combining it with the typical renewal approach used for stochastic resetting,[51] we study the interplay of resetting and self-propulsion. In particular, at the resetting event the agent is reset to its initial configuration, comprising its position and orientation. Our main results suggest that, owing to the strong dependence on the initial orientation, resetting in active motion can either increase or decrease the reset-enabled MFPT to reach the absorbing boundary in comparison to the passive case. Notably, we measure this

[a] *Max-Planck-Institut für Physik komplexer Systeme, Nöthnitzer Straße 38, 01187 Dresden, Germany. E-mail: baouche@pks.mpg.de, ckurzthaler@pks.mpg.de*
[b] *Center for Systems Biology Dresden, Pfotenhauerstraße 108, 01307 Dresden, Germany*
[c] *Cluster of Excellence, Physics of Life, TU Dresden, Arnoldstraße 18, 01062 Dresden, Germany*

directional bias through an anisotropy function and find that it becomes most pronounced when the initial distance to the wall is comparable to the distance traveled by the agent before being reset.

This paper is organized as follows: in Section II we first introduce our model. We then summarize the perturbative approach used to study the FPT statistics of an ABP without stochastic resetting and, using a renewal approach, we link the survival probabilities with and without stochastic resetting. This framework allows us to analytically compute various statistical indicators, including the MFPT, the median, and the skewness, and we finally resolve the full survival probability and FPT probability density, which we present in Section III. We summarize and conclude in Section IV.

II. Model

In this section, we outline the strategy employed to obtain the first-passage-time (FPT) statistics of an active Brownian particle (ABP), whose position and orientation are reset to their initial state at random times. We consider an ABP moving in a two-dimensional (2D) plane (O, x, z). The particle moves at a constant speed v along its instantaneous orientation $\boldsymbol{e}(\vartheta(t)) = (\sin(\vartheta(t)), \cos(\vartheta(t)))$, where $\vartheta(t)$ denotes the polar angle [Fig. 1 (inset)]. The agent undergoes both random translational and rotational motion, characterized by their respective diffusion coefficients D and D_{rot}. In addition, the instantaneous position $\boldsymbol{r}(t)$ and orientation $\vartheta(t)$ are randomly reset to the initial position $\boldsymbol{r}_0 \equiv \boldsymbol{r}(0)$ and orientation $\vartheta_0 \equiv \vartheta(0)$; the resetting events happen at times drawn from an exponential distribution $\phi(t) = \lambda \exp(-\lambda t)$ with rate λ (and mean time between resets $1/\lambda$) (see Fig. 1). These processes are represented by the following set of stochastic equations:

$$\frac{\mathrm{d}\boldsymbol{r}}{\mathrm{d}t} = v\boldsymbol{e} + \sqrt{2D}\boldsymbol{\eta}, \tag{1a}$$

$$\frac{\mathrm{d}\vartheta}{\mathrm{d}t} = \sqrt{2D_{\mathrm{rot}}}\xi, \tag{1b}$$

$$\boldsymbol{r} \to \boldsymbol{r}_0 \text{ and } \vartheta \to \vartheta_0 \text{ with } T(t), \tag{1c}$$

where $\boldsymbol{\eta}(t)$ and $\xi(t)$ are independent Gaussian white noises of zero mean and delta-correlated variance, $\langle \eta_i(t)\eta_j(t')\rangle = \delta_{ij}\delta(t-t')$ for $i,j \in \{1,2\}$ and $\langle \xi(t)\xi(t')\rangle = \delta(t-t')$. Rescaling the position $\boldsymbol{r} = a\boldsymbol{\mathcal{R}}$ with the particle's hydrodynamic radius a and the time $t = \tau T$ with the diffusive time $\tau = a^2/D$, two non-dimensional numbers appear: $\mathrm{Pe} = va/D$ denotes the Péclet number, measuring the relative importance of active motion *versus* diffusion, and $\Lambda = \lambda\tau$ is the reduced resetting rate, representing the prevalence of resetting events compared to the diffusive time scale. We further introduce $\gamma = \tau D_{\mathrm{rot}} = 3/4$, which follows from the Stokes–Einstein–Sutherland relation for a spherical particle. The latter lets us interpret the reduced resetting rate as a competition between resetting and rotational diffusion $\Lambda = 3\lambda/4D_{\mathrm{rot}}$.

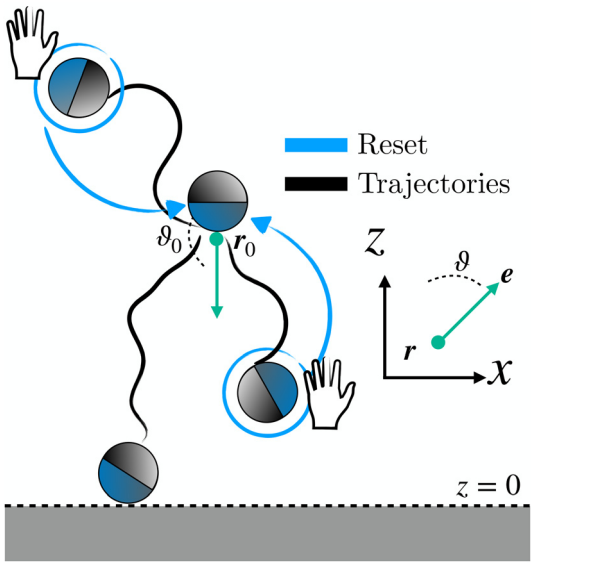

Fig. 1 Schematic of the motion of an ABP under stochastic resetting to its initial position $\boldsymbol{r}_0$ and orientation ϑ_0 near an absorbing boundary at $z = 0$. The green dot and arrow represent the resetting position and orientation, respectively. The inset depicts the agent's position $\boldsymbol{r}$ and orientation ϑ.

A. Renewal framework

To make analytical progress, we rely on a renewal approach for the survival probability $S(T|Z_0,\vartheta_0)$, *i.e.* the probability that the agent, which has started at position Z_0 with orientation ϑ_0, has not yet reached the boundary at time T. Note that we have integrated over the X-direction due to the invariance in the direction parallel to the wall. For exponentially distributed resetting times $\phi(T) = \Lambda \exp(-\Lambda T)$, the survival probability follows:[51]

$$S(T|Z_0,\vartheta_0) = \mathrm{e}^{-\Lambda T} S^{\mathrm{o}}(T|Z_0,\vartheta_0) + \int_0^T \Lambda \mathrm{e}^{-\Lambda T} S^{\mathrm{o}}(T'|Z_0,\vartheta_0) S(T-T'|Z_0,\vartheta_0)\mathrm{d}T', \tag{2}$$

where $S^{\mathrm{o}}(T'|Z_0,\vartheta_0)$ corresponds to the survival probability of an ABP in the absence of resetting. Eqn (2) is to be interpreted in the following way: the probability to survive up to time T is the sum of the probability to survive up to time T without any resetting event and the sum over the probabilities to survive up to time T' given a reset at an earlier time $T - T'$. The survival probability provides access to the FPT probability density $F(T|Z_0,\vartheta_0)$, characterizing the distribution of times at which the agent reaches the wall:

$$F(T|Z_0,\vartheta_0) = -\frac{\mathrm{d}}{\mathrm{d}T} S(T|Z_0,\vartheta_0). \tag{3}$$

To compute the survival probability we employ a Laplace transform $T \mapsto s$

$$\hat{S}(s|Z_0,\vartheta_0) = \int_0^\infty S(T|Z_0,\vartheta_0)\mathrm{e}^{-sT}\mathrm{d}T, \tag{4}$$

which allows us to readily obtain a closed-form solution

$$\hat{S}(s|Z_0,\vartheta_0) = \frac{\hat{S}^{\mathrm{o}}(s+\Lambda, Z_0, \vartheta_0)}{1-\Lambda\hat{S}^{\mathrm{o}}(s+\Lambda, Z_0, \vartheta_0)}. \tag{5}$$

It then suffices to know $\hat{S}^{\mathrm{o}}$ – the survival probability without resetting – to obtain the survival probability with resetting $\hat{S}$ in Laplace space.

The former quantity was the object of our previous work,[52] where we have derived analytical expressions for S^{o} through a perturbation expansion for small Péclet numbers. While details of the perturbation expansion can be found in ref. 52 and Appendix A, we recapitulate the most important steps here. Starting from eqn (1a) and (1b), we first derive a (non-dimensional) Fokker–Planck equation for the probability density $\mathbb{P}^{\mathrm{o}}(\boldsymbol{\mathcal{R}}, \vartheta, T|\boldsymbol{\mathcal{R}}_0, \vartheta_0)$ of a particle to be at $\boldsymbol{\mathcal{R}}$ with orientation ϑ at time T having started at $\boldsymbol{\mathcal{R}}_0$ with orientation ϑ_0 at $T = 0$:

$$\partial_T\mathbb{P}^{\mathrm{o}} = -\mathrm{Pe}\ \boldsymbol{e}\cdot\boldsymbol{\nabla}\mathbb{P}^{\mathrm{o}} + \gamma\partial_\vartheta{}^2\mathbb{P}^{\mathrm{o}} + \nabla^2\mathbb{P}^{\mathrm{o}}. \tag{6}$$

Since the boundary is infinite in the X direction, we further integrate out the X component and arrive at

$$\partial_T\mathbb{P}^{\mathrm{o}} = -\mathrm{Pe}\cos(\vartheta)\partial_Z\mathbb{P}^{\mathrm{o}} + \gamma\partial_\vartheta{}^2\mathbb{P}^{\mathrm{o}} + \partial_Z{}^2\mathbb{P}^{\mathrm{o}}, \tag{7}$$

which is supplemented by the following initial and boundary conditions:

$$\mathbb{P}^{\mathrm{o}}(Z,\vartheta,T=0|Z_0,\vartheta_0) = \delta(Z-Z_0)\delta(\vartheta-\vartheta_0), \tag{8a}$$

$$\mathbb{P}^{\mathrm{o}}(Z=0,\vartheta,T|Z_0,\vartheta_0) = 0 \quad \forall T\in\mathbb{R}^+. \tag{8b}$$

Next, we move to Laplace space ($s \mapsto T$) and thus eqn (7) transforms to

$$(s-\mathcal{H})\widehat{\mathbb{P}}^{\mathrm{o}} = \delta(Z-Z_0)\delta(\vartheta-\vartheta_0), \tag{9}$$

where the operator $\mathcal{H} \equiv \mathcal{H}_0 + \mathrm{Pe}\,\mathcal{V}$ is split into two components: the unperturbed operator $\mathcal{H}_0 \equiv \gamma\partial_\vartheta{}^2 + \partial_Z{}^2$ and the perturbation $\mathcal{V} \equiv -\cos(\vartheta)\partial_Z$. Expanding the probability density in terms of the Péclet number

$$\widehat{\mathbb{P}}^{\mathrm{o}} = \widehat{\mathbb{P}}^{\mathrm{o}}_0 + \mathrm{Pe}\ \widehat{\mathbb{P}}^{\mathrm{o}}_1 + \mathrm{Pe}^2\ \widehat{\mathbb{P}}^{\mathrm{o}}_2 + \mathcal{O}(\mathrm{Pe}^3), \tag{10}$$

and inserting it into eqn (9), leads to a set of coupled equations for the perturbations [eqn (A1a)–(A1c) in Appendix A]. Analytical expressions for $\widehat{\mathbb{P}}^{\mathrm{o}}_k$ can be obtained iteratively and used as input for the survival probability $\hat{S}^{\mathrm{o}}(s|Z_0,\vartheta_0) = \sum_{n=0}^{\infty}\mathrm{Pe}^n\ \hat{S}^{\mathrm{o}}_n(s|Z_0,\vartheta_0)$ *via* the relation

$$\hat{S}^{\mathrm{o}}_n(s|Z_0,\vartheta_0) = \int_0^\infty \widehat{\mathbb{P}}^{\mathrm{o}}_n(s,Z|Z_0,\vartheta_0)\mathrm{d}Z. \tag{11}$$

Analytical predictions up to second order in the Pe number can be found in the Appendix A. Finally, inserting the small-Pe expansion of $\hat{S}^{\mathrm{o}}(s|Z_0,\vartheta_0)$ into eqn (5) yields the survival probability in the presence of stochastic positional and orientational resetting $\hat{S}(s|Z_0,\vartheta_0)$ and provides immediate access to the FPT probability density.

To further quantify the FPT properties, we are interested in the low-order moments of the first-passage times, which are accessible through the survival probability in Laplace space $\hat{S}$. In particular, the n-th moment of the random variable F_T associated with the FPT probability density can be obtained *via*

$$\mathbb{E}\left[F_T^n\right] = \int_0^\infty T^n F(T|Z_0,\vartheta_0)\mathrm{d}T, \tag{12a}$$

$$= -\int_0^\infty T^n\left(\frac{\mathrm{d}}{\mathrm{d}T}S(T|Z_0,\vartheta_0)\right)\mathrm{e}^{-sT}\big|_{s=0}\mathrm{d}T, \tag{12b}$$

$$= (-1)^{n+1}\frac{\mathrm{d}^n}{\mathrm{d}s^n}\left[s\hat{S}(s|Z_0,\vartheta_0)\right]_{s=0}, \tag{12c}$$

where we have used the relation between $F(T|Z_0,\vartheta_0)$ and $S(T|Z_0,\vartheta_0)$ [eqn (3)] and the properties of the Laplace transform.

B. Expansion in the Péclet number

Note that we can further expand the survival probability for small Pe, $\hat{S}(s|Z_0,\vartheta_0) = \sum_{n=0}^{\infty}\mathrm{Pe}^n\ \hat{S}_n(s|Z_0,\vartheta_0)$ [eqn (5)], and formally obtain the associated coefficients:

$$\hat{S}_0 = \frac{\hat{S}^{\mathrm{o}}_0}{1-\Lambda\hat{S}^{\mathrm{o}}_0}, \tag{13a}$$

$$\hat{S}_1 = \frac{\hat{S}^{\mathrm{o}}_1}{1-\Lambda\hat{S}^{\mathrm{o}}_0} + \frac{\Lambda\hat{S}^{\mathrm{o}}_0\hat{S}^{\mathrm{o}}_1}{\left(1-\Lambda\hat{S}^{\mathrm{o}}_0\right)^2}, \tag{13b}$$

$$\hat{S}_2 = \frac{\hat{S}^{\mathrm{o}}_2}{1-\Lambda\hat{S}^{\mathrm{o}}_0} + \frac{\Lambda\left(\hat{S}^{\mathrm{o}}_0\hat{S}^{\mathrm{o}}_2 + \left(\hat{S}^{\mathrm{o}}_1\right)^2\right)}{\left(1-\Lambda\hat{S}^{\mathrm{o}}_0\right)^2} + \frac{\Lambda^2\hat{S}^{\mathrm{o}}_0\left(\hat{S}^{\mathrm{o}}_1\right)^2}{\left(1-\Lambda\hat{S}^{\mathrm{o}}_0\right)^3}, \tag{13c}$$

which can be readily extended to higher orders. Using this result, the FPT probability density in Laplace space obeys

$$\hat{F}(s|Z_0,\vartheta_0) = 1 - s\hat{S}_0(s|Z_0,\vartheta_0) - s\sum_{n=1}^{\infty}\mathrm{Pe}^n\ \hat{S}_n(s|Z_0,\vartheta_0), \tag{14}$$

where the first two terms correspond to the FPT probability density of a Brownian particle under stochastic resetting and the sum encodes the effect of activity.

C. Brownian particle under stochastic resetting

Our framework allows recovering the well-established result for the survival probability of a passive Brownian particle under stochastic resetting as

$$\hat{S}_0(s|Z_0,\vartheta_0) = \frac{1-\mathrm{e}^{-\sqrt{\Lambda+s}Z_0}}{s+\Lambda\mathrm{e}^{-\sqrt{\Lambda+s}Z_0}}. \tag{15}$$

Notably, we mentioned that introducing a resetting mechanism for a diffusive process establishes a finite mean first-passage time (MFPT). It reduces to

$$\mathbb{E}[F_T]_{\mathrm{B}} = \hat{S}_0(s=0) = \frac{\mathrm{e}^{\sqrt{\Lambda}Z_0}-1}{\Lambda}, \tag{16}$$

which represents the well-known MFPT for a diffusive particle under stochastic positional resetting.[1] It diverges as $\propto \Lambda^{-1/2}$ for $\Lambda \to 0$, thus approaching the behavior of a Brownian

particle without resetting. Furthermore, it diverges as $\Lambda \to \infty$, reflecting the particles that are constantly reset and never manage to reach the wall. Most importantly, for a fixed initial distance Z_0, there exists an optimal resetting rate $\Lambda_B^* = (Z^*)^2/Z_0^2$ that minimizes the MFPT, where $Z^* = 1.59362\ldots$ is the unique solution of the transcendental equation:

$$\frac{Z^*}{2} = 1 - \mathrm{e}^{-Z^*}. \tag{17}$$

This indicates that minimizing the MFPT far away from the wall requires resetting the agent less often.

III. Results

In what follows, we show our results for the active Brownian particle under stochastic resetting by expanding $\hat{S}^{\mathrm{o}}$ up to the second order in the Péclet number. We discuss the mean first-passage times [Section III A], the optimal resetting rate [Section III B], the anisotropy of the process [Section III C], the survival probability and the probability density for the FPT [Section III D], as well as the skewness and the median of the FPTs [Section III E and F].

A. Mean first-passage time

We compute the mean first-passage time (MFPT) by following the strategy outlined in Section II A. Our theoretical prediction reveals that it becomes finite [eqn (B1) in Appendix B] within the limit of small Pe and depends strongly on the initial orientation ϑ_0 and initial distance to the boundary z_0. Let us first note that Fig. 2(A)–(C) show that our theoretical predictions are nicely corroborated by simulation results (see Appendix D for details). We further note that though our results may loose accuracy for Pe $\geq$ 1, we show in Appendix C that our perturbation approach remains valid for this parameter range and we observe very good agreement with simulations even at larger Péclet numbers.

Importantly, we find that an agent initially facing the wall ($\vartheta = \pi$) reaches it faster than an agent oriented away from the wall ($\vartheta = 0$), which is in turn slower than a diffusive agent [Fig. 2(A) and (B)]. Assuming uniformly distributed initial angles leads to a slightly lower MFPT than the diffusive case [Fig. 2(C)]. Additionally, increasing activity through the Péclet number expedites and delays the arrival at the boundary for $\vartheta_0 = \pi$ and $\vartheta_0 = 0$, respectively. This is explained by the fact that the distance the particle travels before reorienting (*i.e.*, the persistence length) increases conjointly with activity, $l_{\mathrm{p}} = v/D_{\mathrm{rot}} = a\mathrm{Pe}/\gamma$, and that the agent's initial orientation is also reset in the process. Hence, a particle initially departing from (respectively moving towards) the wall at a higher velocity will reach the wall at later (respectively earlier) times even with resetting. Importantly, the divergence of the MFPT $\propto \Lambda^{-1/2}$ as $\Lambda \to 0$ and for $\Lambda \to \infty$ is preserved for an active particle, as resetting too often prevents ever reaching the wall and not resetting enough leads to the

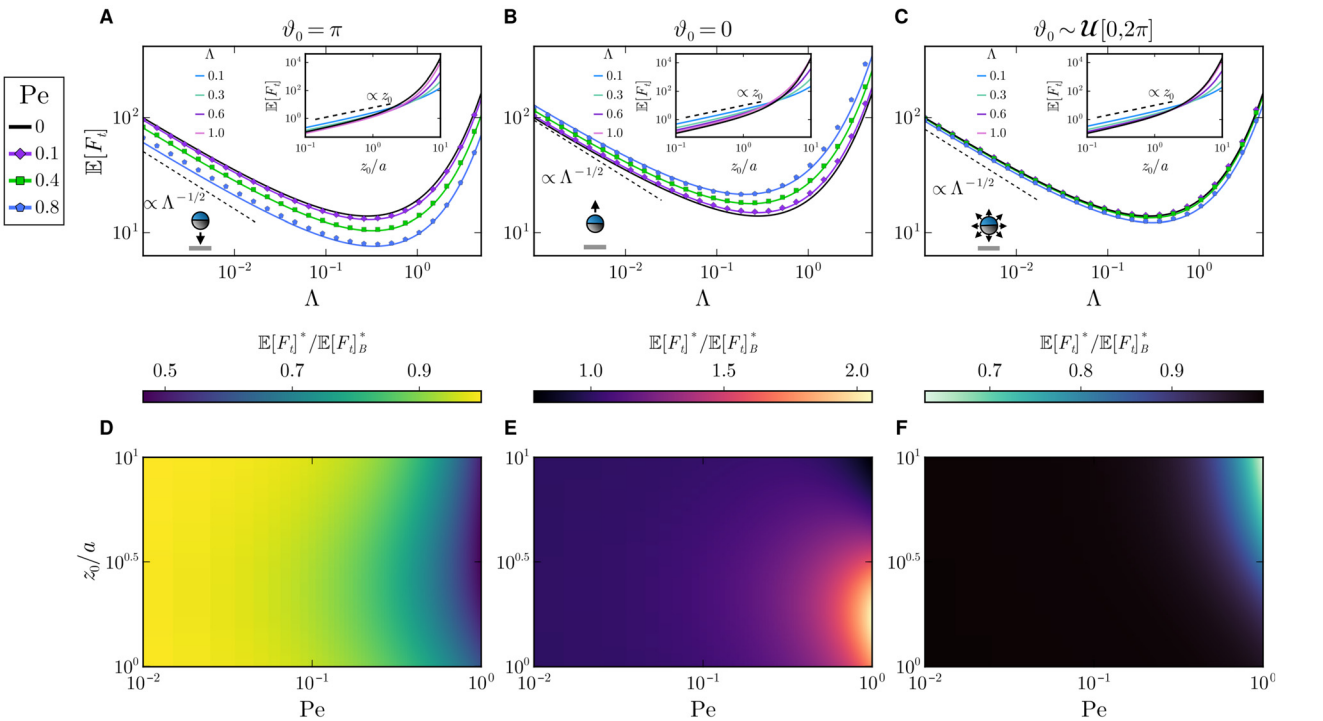

Fig. 2 (A)–(C) Mean first-passage time $\mathbb{E}[F_t]$ for three different initial angles ϑ_0 as a function of the resetting rate Λ (with $z_0/a = 3$) for different Péclet numbers Pe. Insets show the MFPT as a function of the initial distance z_0 for several Λ and Pe = 0.5. (D)–(F) Ratio of the mean first-passage times of an active and passive Brownian particle at the optimal resetting rate $\mathbb{E}[F_t]^*/\mathbb{E}[F_t]^*_{\mathrm{B}}$ as a function of Pe and z_0. Columns show results for particles (A) and (D) initially facing the wall, (B) and (E) initially facing against the wall, and (C) and (F) with initial angles drawn from a uniform distribution $\mathcal{U}[0, 2\pi]$. Solid lines and markers denote theory and simulations, respectively. The black lines in (A)–(C) correspond to the passive case with resetting rate $\Lambda_B = 1$.

divergence as for a simple ABP. We can expect this scaling to change for higher activity, as persistent motion will dictate short-time dynamics.

The MFPTs further depend on the agent's initial distance z_0 [Fig. 2(A)–(C) (insets)]. In particular, they increase linearly in z_0 for short distances $z_0/a \lesssim 1$, in agreement with the passive case and irrespective of ϑ_0 and Λ. Increasing Λ expedites the process for short initial distances $z_0/a \lesssim 1$. At large distances $z_0/a \gtrsim 1$ the MFPTs diverge, which occurs earlier for small Λ. Thus, independent of the initial orientation ϑ_0 resetting more frequently at short distances z_0 is more efficient than at large z_0. This can be rationalized as follows: when the time between resets becomes shorter than the time it takes the agents to reach the wall, it becomes impossible for particles to reach the wall and thus the MFPT diverges. Fixing the resetting rate for the passive case to $\Lambda = 1$ and comparing it to the active case with the same rate shows that at large z_0 the active agent is always faster ($\vartheta_0 = \pi$, $\vartheta_0 \sim \mathcal{U}[0, 2\pi]$) or takes about an equal amount of time ($\vartheta_0 = 0$) to reach the wall.

Our results demonstrate that the MFPTs exhibit a minimum as a function of Λ [Fig. 2(A)–(C)], which begs the question of the optimal MFPT $\mathbb{E}[F_t]^*$ (and corresponding resetting rate Λ^*) to accelerate absorption at the boundary. We begin this discussion by comparing $\mathbb{E}[F_t]^*$ with its passive counterpart $\mathbb{E}[F_t]^*_{\mathrm{B}}$ [Fig. 2(D)–(F)]. For low activity Pe $\lesssim 0.1$, the active and passive cases are comparable, $\mathbb{E}[F_t]^*/\mathbb{E}[F_t]^*_{\mathrm{B}} \approx 1$, and the initial angle remains unimportant. Deviations appear as Pe increases and approaches one, where agents initially oriented towards the wall always display a lower optimal MFPT. However, agents departing away from it exhibit a slightly more complex behavior: at short initial distances $z_0/a \lesssim 3$, they are naturally slower $\mathbb{E}[F_t]^*/\mathbb{E}[F_t]^*_{\mathrm{B}} \approx 2$ because of the persistent motion, but as $z_0/a \to 10$, rotational diffusion kicks in and allows agents to reorient and move persistently towards the boundary, which makes them faster than diffusive particles (see also inset of Fig. 2B). For the same reason, randomly initially oriented particles will reach the boundary faster when both activity and initial position are large enough.

Overall, for particles facing the wall and randomly oriented particles, the optimal MFPT decreases as a function of Pe for any z_0, while particles facing away from the wall exhibit an increase of their optimal MFPT with activity, except when the initial distance is sufficiently large, in which case this trend does not hold [Fig. 3].

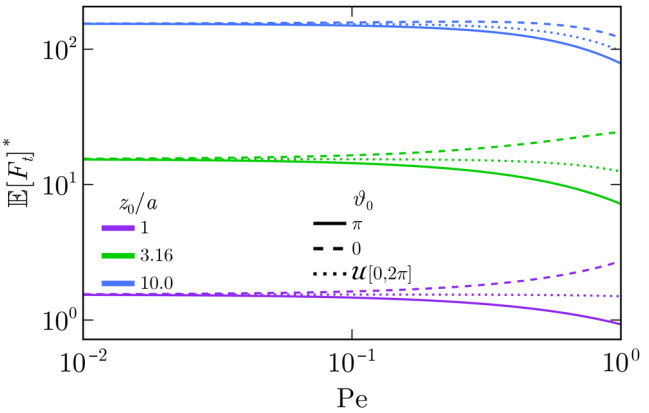

Fig. 3 Optimal MFPT $\mathbb{E}[F_t]^*$ as a function of the Péclet number Pe for several initial distances z_0/a. The solid lines correspond to $\vartheta_0 = \pi$, dashed lines to $\vartheta_0 = 0$ and dotted lines to an initial angle randomly chosen.

B. Optimal resetting rate

Next, we are interested in what determines this optimal resetting rate and since trying to solve analytically for Λ^* leads to a lengthy transcendental equation, we rather rely on numerics and compare it with the passive case Λ^*_B in Fig. 4. In agreement with our observation for the optimal MFPT, the initial angle appears irrelevant for small Pe $\lesssim 0.1$, thus leading to $\Lambda^*/\Lambda^*_B \simeq 1$.

The optimal resetting rate Λ^* for a particle facing the wall ($\vartheta_0 = \pi$) displays two behaviors depending on the initial distance: for $z_0/a \simeq 1$ the optimal rate Λ^* decreases with Péclet number, as letting the particle reach the boundary through persistent motion is the most effective strategy. In particular, resetting as often as in the passive case would take the particle away from the boundary and increase the FPT. However, at larger initial distances, Λ^* becomes larger than the passive counterpart and increases with activity. Thus, active particles need to be reset more often as they can reorient due to rotational motion, which enables them to move away from the boundary. Furthermore, Λ^*/Λ^*_B displays a maximum (see first plot in Fig. 4D). The presence of this maximum can be understood by considering the length the agent moves in the z-direction before resetting

$$\begin{aligned} l_{\mathrm{R}} &= \int_0^\infty \langle \Delta z(t)\rangle \lambda \mathrm{e}^{-\lambda t} = \frac{v}{D_{\mathrm{rot}}+\lambda}\cos(\vartheta_0), \\ &= \frac{4a\mathrm{Pe}}{3+4\Lambda}\cos(\vartheta_0), \end{aligned} \tag{18}$$

where $\langle \Delta z(t)\rangle$ is the average displacement at time t[47]

$$\langle \Delta z(t)\rangle = \frac{v}{D_{\mathrm{rot}}}\left(1-\mathrm{e}^{-D_{\mathrm{rot}}t}\right)\cos(\vartheta_0). \tag{19}$$

Eqn (18) represents the persistence length with a contribution of the resetting rate ($D_{\mathrm{rot}} \to D_{\mathrm{rot}} + \lambda$). Thus, as the resetting length and the initial distance become comparable $l_{\mathrm{R}}/z_0 \sim 1$, resetting too often becomes disadvantageous.

For a particle that is facing away from the boundary and for Pe close to one, we distinguish three cases: first, for $z_0/a \simeq 1$, the particle needs to be reset more frequently because of the influence of ϑ_0. In this regime, it is likely that the particle arrives at the wall through translational diffusion, while active motion takes it away. Second, for intermediate z_0/a, resetting events need to be less frequent, to ultimately increase the chances of reorienting through rotational diffusion towards the wall and reaching it *via* active motion. Third and lastly, for $z_0/a \simeq 10$, the agent requires more frequent resets, similar to the case of a particle initially facing the boundary.

Averaging out the effect of the initial orientation ϑ_0 shows that an active particle, as a result of persistent motion, needs to be reset more frequently at larger initial distances and for

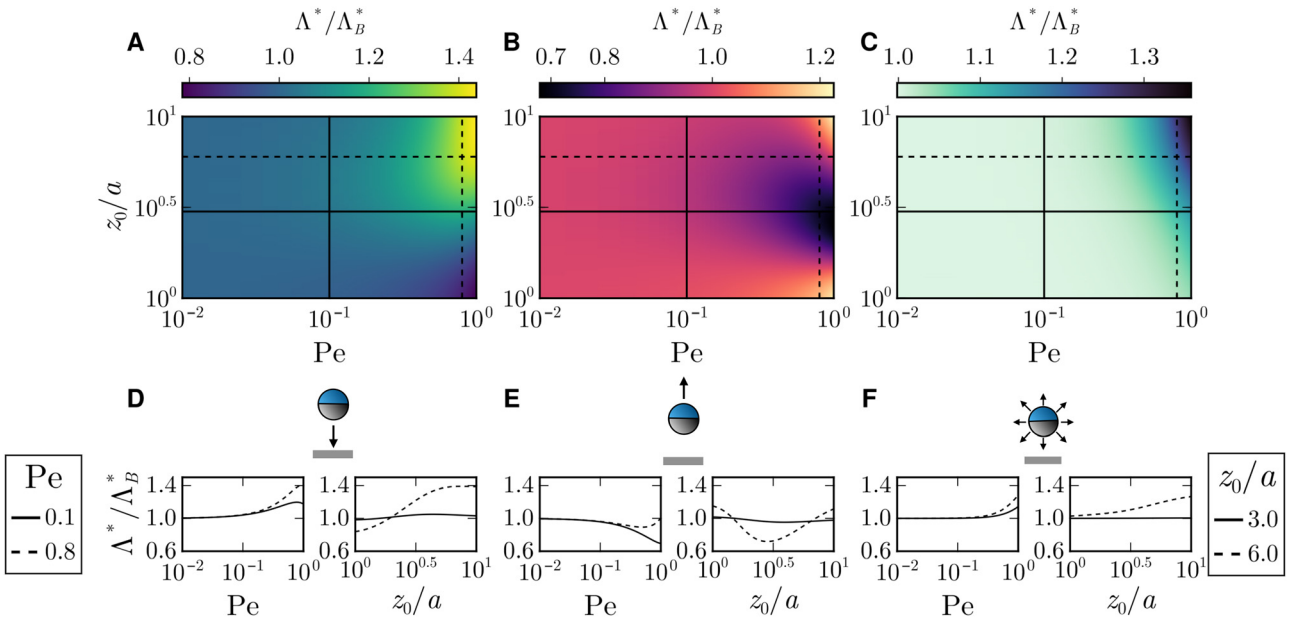

Fig. 4 (A)–(C) Ratio of the optimal resetting rate Λ^*/Λ_B^* for three different initial angles ϑ_0 as a function of the Péclet number Pe and of the initial position z_0/a. (D)–(F) Ratio Λ^*/Λ_B^* as function of Pe (respectively, z_0/a) at fixed z_0/a (respectively, Pe). Columns show results for particles (A) and (D) initially facing the wall, (B) and (E) initially facing against the wall, and (C) and (F) with initial angles drawn from a uniform distribution $\mathcal{U}[0, 2\pi]$.

higher Péclet numbers than the passive counterpart [Fig. 4F]. Interestingly $\Lambda^\star$ seems to have no extremum when the initial angle is randomized, suggesting that resetting more frequently is always an advantage for the parameter range considered.

C. Anisotropy of the mean first-passage time

To further quantify the effect of the initial orientation we introduce the anisotropy function *via*

$$\mathcal{A}(z_0, \vartheta_0) = \frac{\mathbb{E}[F_T](z_0, \vartheta_0)}{\mathbb{E}[F_T](z_0, \vartheta_0 + \pi)}, \tag{20}$$

measuring the ratio of the MFPT given an initial position and orientation with the MFPT given the same initial position but with the diametrically opposed initial orientation. Fig. 5A indicates that the anisotropy for an agent initially oriented towards the wall (respectively opposite to the wall) is large at small initial distances $z_0/a \lesssim 1$ and is a decreasing function of Λ. This is due to the fact that at such distances, the particle initially oriented towards the wall should reach it almost immediately, which is hindered by a too frequent resetting mechanism. For $z_0/a \gtrsim 10$, the anisotropy relaxes to $\mathcal{A}(Z_0, 0) \to 1$, independently of the resetting rate, as the memory of the initial orientation progressively decays for such large initial distances.

At intermediate distances $z_0/a \simeq 1$ the anisotropy exhibits a maximum for large enough resetting rates ($\Lambda \gtrsim 0.1$) which can be rationalized in the following way: at these distances, resetting events start to be prevalent and thus effectively rectify the trajectory of agents that started moving towards the wall but oriented away and the trajectory of agents that departed away from the wall but managed to reorient towards it through rotational diffusion, strengthening the discrepancy in their

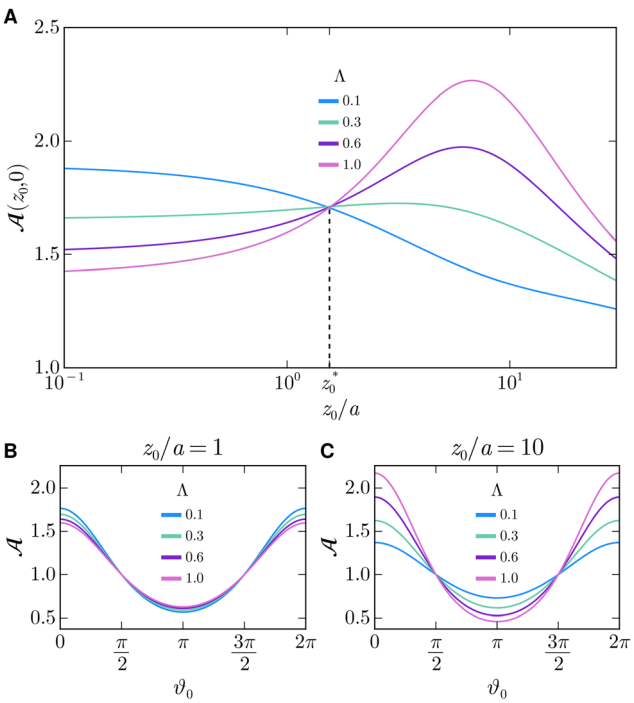

Fig. 5 (A) Anisotropy $\mathcal{A}(z_0, 0)$ as a function of the initial position z_0 for different resetting rates Λ. (B) and (C) Anisotropy as a function of the initial angle ϑ_0 for different Λ and z_0. The Péclet number is Pe = 0.4.

MFPTs. We further note that the maximum displaces towards the right with increasing resetting rate Λ, as the distance $l_R \propto \mathrm{Pe}/\Lambda$ traveled before resetting decreases with Λ.

We note that there is a point z_0^* where the anisotropy appears to be independent of the resetting rate. We anticipate that it

corresponds to the distance when active motion starts to become comparable to translational diffusion. Comparing the length traveled through diffusion during time t ($l^2 = tD$) with the length traveled using active motion ($l = tv$) leads to $l = a/\mathrm{Pe}$, which predicts the disappearance of that point at larger Pe. This feature remains to be further studied for larger Péclet numbers that go beyond our perturbation limits.

Finally, we study how the anisotropy behaves as a function of the initial angle. It is maximal for $\vartheta_0 = 0, 2\pi$, since the median FPT of agents initially moving away from the wall is greater than that of agents going to the wall. Reciprocally, it is minimal for $\vartheta_0 = \pi$. Since translation diffusion plays a major role for small initial distances, the importance of the resetting rate is minimal [Fig. 5B] for small z_0/a. As the initial distance gets larger, the particle takes more and more advantage of persistent motion and the anisotropy thus increases [Fig. 5C]. Most importantly, it becomes larger for increasing Λ, compared to smaller z_0, where a reduced rate Λ produces the largest anisotropy. Thus the curves intersect at an intermediate distance z_0^*.

D. Survival probability and first-passage-time distribution

In the past section, we studied the MFPT, which gave us a quantitative answer to the question of "speed of completion". We can now try to deepen our understanding by also computing the survival probability $S(t|z_0,\vartheta_0)$ and the FPT probability density function $F(t|z_0,\vartheta_0)$. Fig. 6(A)–(C) shows an exponential decay for the survival probability, independently of the initial angle. Thus, resetting profoundly changes the power-law behavior $\sim t^{-1/2}$ of a simple ABP at low Pe,[52] which remains visible for times $t/\tau \leq \Lambda^{-1}$, as resetting has not yet settled in [Fig. 6(A)–(C) (inset)]. The absence of this power-law tail is a sign that, unlike the non-resetting case, agents manage to reach the wall within a finite time due to the resets to their initial configuration.

As we resolve the distributions for distances larger than the agent's persistence length, $z_0/a = 3 \gtrsim l_\mathrm{p}/a$, rotational diffusion plays an important role. Thus, the question of which survival distribution decays faster depending on Λ follows the same logic as for the optimal MFPT: resetting is an advantage if it resists departure from the wall without hindering reorientation towards it ($\vartheta_0 = 0$), while at the same time ensuring that there is enough time to reach it ($\vartheta_0 = \pi$). Furthermore, we note that the optimal resetting rate is $\Lambda^* \approx 0.3$ for all cases, which is reflected in the fact that the survival decays the fastest for $\Lambda = 0.3$.

We further comment on the behavior of the survival probability at large distances $z_0/a \gg l_\mathrm{p}$. In free space, it is well-established that at large times $t \gtrsim 1/D_\mathrm{rot}$ an ABP enters an effective diffusive regime characterized by the effective diffusion coefficient

$$D_\mathrm{eff} = D\left(1 + \frac{2}{3}\mathrm{Pe}^2\right). \tag{21}$$

We therefore suggest that an active particle, which starts far away from the boundary, reaches the wall through effective diffusion. Thus, its survival probability in this regime assumes the form of that of a Brownian particle in eqn (15) by replacing

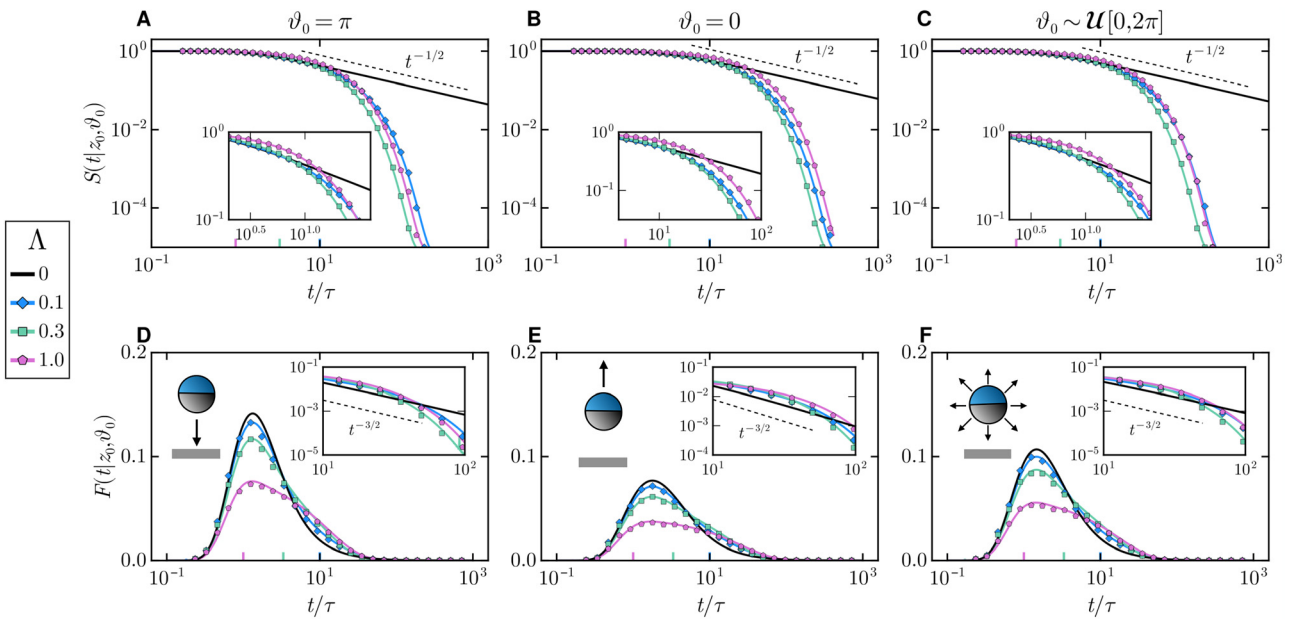

Fig. 6 Survival probability (A)–(C) and FPT probability density (D)–(F) as a function of time t for three different initial angles ϑ_0: the particle is initially (A) facing the wall, (B) facing against the wall, and (C) randomly oriented with an angle drawn from a uniform distribution $\mathcal{U}[0,2\pi]$. Here, the initial position is $z_0/a = 3$ and the Péclet number is $\mathrm{Pe} = 0.4$. Solid lines and symbols denote theory and simulations for different resetting rates, respectively. The black lines represent the active case in the absence of resetting. The insets show a zoomed-in region of the plot containing them. The colored vertical lines represent the typical resetting times $1/\Lambda$.

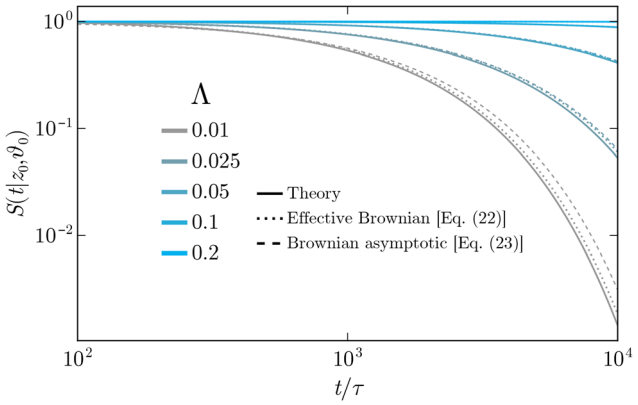

Fig. 7 Survival probability $S(t|z_0,\vartheta_0)$ of an active particle for different resetting rates Λ. The solid lines correspond to the perturbation theory, the dotted lines represent the prediction for the effective Brownian case [eqn (22)] and the dashed lines the associated asymptotic approximation [eqn (23)]. Here, the initial distance is $z_0/a = 30$, the initial orientation is $\vartheta_0 = \pi$, and the Péclet number is Pe = 0.4.

the translational diffusivity D by the effective diffusivity D_{eff}:

$$\hat{S}(s|z_0) = \frac{1 - e^{-\sqrt{(\lambda+s)/D_{\text{eff}}}z_0}}{s + \lambda e^{-\sqrt{(\lambda+s)/D_{\text{eff}}}z_0}}. \tag{22}$$

In the time variable, the latter has the following asymptotic behavior[1]

$$S(t|z_0) \simeq e^{-\lambda t e^{-\sqrt{\lambda/D_{\text{eff}}}z_0}} \text{ for } \sqrt{\lambda/D_{\text{eff}}}z_0 \gg 1. \tag{23}$$

We observe that for Pe = 0.4, the survival probability at long times is well approximated by that of a passive agent under resetting performing effective diffusion [dotted lines in Fig. 7]. The asymptotic prediction in eqn (23) also nicely agrees with our findings, highlighting the exponential tails of the survival probability at long times. In our previous work,[52] we have demonstrated that the memory of the initial angle is never actually lost and that the amplitude of the tail of the survival probability in the absence of resetting depends non-trivially on the original orientation. Introducing the resetting smoothens this effect but deviations from the passive case are naturally expected to increase with the Péclet number.

Putting in parallel the survival probability with the FPT probability density [Fig. 6(D)–(F)] shows that a faster decay of S leads to a faster-decaying tail for F, where again no power-law $F \propto t^{-3/2}$ is present, as in the absence of resetting.[52] Finally, we observe that even though the resetting mechanism annihilates the tail, increasing the rate causes the distribution to flatten and spread over at intermediate times $0.1 \lesssim t/\tau \lesssim 100$. Resetting the particle often enables situations where it reaches the wall after longer times due to the large number of resets. To expand on this observation, we compute another statistical quantity, the skewness.

E. Skewness of the distribution

Given the shape of the FPT probability density, we compute the skewness, measuring the asymmetry around the MFPT. The skewness is defined as the third standardized moment:

$$\tilde{\mu}_3 = \frac{\mathbb{E}\left[(F_T - \mathbb{E}[F_T])^3\right]}{\mathbb{E}\left[(F_T - \mathbb{E}[F_T])^2\right]^{3/2}}, \tag{24}$$

where we use eqn (12c) to obtain the moments. The results are summarized in Fig. 8A where we plot $\tilde{\mu}_3$ as a function of Λ for several z_0. We first note that the skewness is positive for all cases, indicating that the FPT distribution is right-skewed, or skewed towards the large arrival times, accounting for the agents that manage to reach the wall at later times $t/\tau \gg 1$. It also diverges for vanishing Λ, in accordance with the absence of moments for the non-resetting case. For a fixed z_0/a, the skewness decreases when Λ increases, which is consistent with

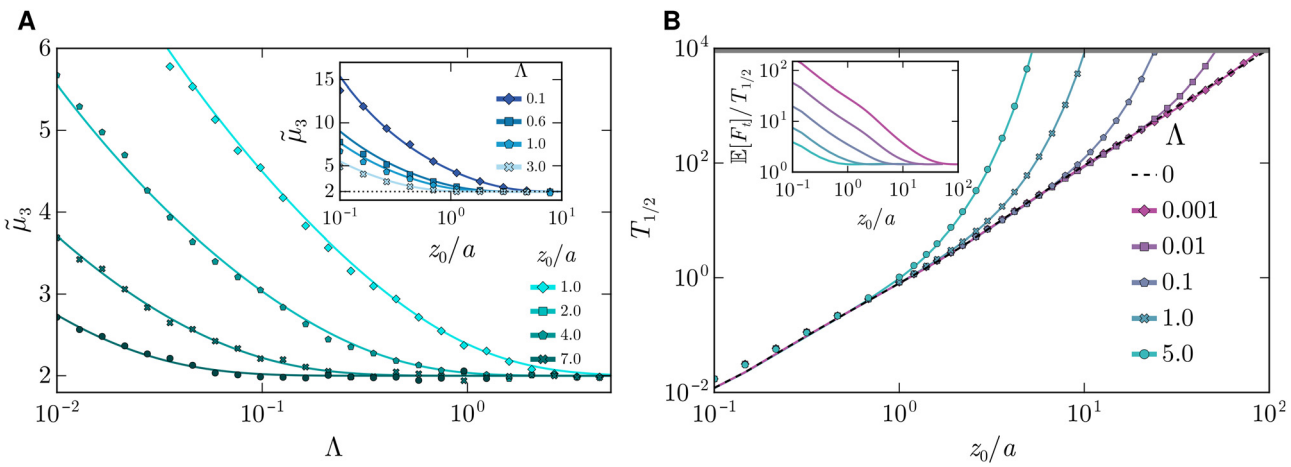

Fig. 8 (A) Skewness $\tilde{\mu}_3$ as a function of the reduced resetting rate Λ for different initial positions z_0 and (inset) as a function of z_0 for different Λ. The Péclet number is Pe = 0.4 and initial orientation $\vartheta_0 = \pi$. Theory and simulations are shown with solid lines and markers, respectively. (B) Median $T_{1/2}$ as a function of the initial position z_0 for different reduced resetting rates Λ. The initial angle is $\vartheta_0 = \pi$ and the Péclet number is Pe = 0.4. Theory and simulations are shown with solid lines and markers, respectively. The shaded gray corresponds to the simulation time limit. (inset) Shows the ratio of the MFPT and the median as a function of z_0/a.

the observation that the FPT probability density for $z_0/a = 3$ stretches over a broader range of times. If the particle is increasingly reset, it naturally requires more attempts and thus time to successfully reach the wall.

Interestingly, the skewness converges to 2 when the initial position is large $z_0/a \gg 1$ (independently of Λ) or when the resetting rate is large $\Lambda > 1$ (independently of z_0). Based on our analysis of the optimal MFPT and optimal resetting rate, we expect that the skewness should converge to that of the resetting effective Brownian case. Using eqn (24) with the leading-order term $\hat{S}_0$ provides the skewness of the FPT probability density of a Brownian particle under stochastic resetting

$$\tilde{\mu}_3^B = \frac{-8 + e^{\sqrt{\Lambda}Z_0}\left(8e^{2\sqrt{\Lambda}Z_0} - 3\sqrt{\Lambda}Z_0 - 12e^{\sqrt{\Lambda}Z_0}\sqrt{\Lambda}Z_0 + 3\Lambda {Z_0}^2\right)}{4\left(-1 + e^{2\sqrt{\Lambda}Z_0} - e^{\sqrt{\Lambda}Z_0}\sqrt{\Lambda}Z_0\right)^{3/2}}, \tag{25}$$

which converges to 2 for $\sqrt{\Lambda}Z_0 \to \infty$, thus explaining the behavior of the skewness for the FPT probability of an active agent.

F. Median of the first-passage time

For the sake of completeness we further compute the median $T_{1/2}$, giving the value that splits the distribution into two equiprobable parts and defined as:

$$\int_0^{T_{1/2}} F(T|Z_0, \vartheta_0)\mathrm{d}T = \frac{1}{2}. \tag{26}$$

In the non-resetting case, where the MFPT is not defined, the median allowed us to give a quantitative answer to the question of the FPT,[52] which we compare here to the resetting case. Fig. 8B displays the median $T_{1/2}$ as a function of the initial position z_0 for several rates Λ and for $\vartheta_0 = \pi$. In the case of no resetting and very low resetting rate $\Lambda \ll 1$, the median grows quadratically with the initial distance $T_{1/2} \propto {z_0}^2$ (as the diffusive case). For increasing Λ, $T_{1/2}$ starts to diverge at $z_0/a \gtrsim 10$, as the positional resetting events are too frequent for the agent to ever reach the wall.

To further quantify the (a)symmetry of the distribution, we compare the ratio of the mean and the median in Fig. 8A (inset). At small initial distances $z_0/a \lesssim 1$, we first notice that for vanishing Λ, the ratio $\mathbb{E}[F_t]/T_{1/2}$ diverges since the MFPT itself diverges while the median remains defined. As the resetting rate increases, $\mathbb{E}[F_t]/T_{1/2}$ decreases due to the resetting process stabilizing the distribution. We finally note that even though both the median and the MFPT diverge at large z_0/a, their ratio seems to eventually converge to a value slightly above one, independently of the resetting rate, which is consistent with the positive skewness studied in the previous section. Thus, this further emphasizes that the distribution remains asymmetric for any parameters considered here. (Let us finally note that the results remain qualitatively similar for different initial orientations.)

IV. Conclusion

Here, we have studied the FPT properties of an ABP under stochastic resetting to its initial configuration. Employing a previously developed perturbative approach and a renewal framework, we compute exact expressions for the FPT probability density and several other statistical indicators such as the mean, skewness, and median. The main difference to the bare diffusive case is the additional initial orientation of the particle relative to the wall, which can make reaching the boundary slower or faster than a diffusive particle. By quantifying the optimal resetting rate our results demonstrate that active agents, which are relatively far away from the boundary, should be reset more frequently than passive ones to minimize their arrival time, as active motion can take them further away. We further discuss the effect of the initial orientation through an anisotropy function which becomes most pronounced when the initial distance is comparable to the distance the particle travels before it is reset.

The theory developed in this work is valid for small Péclet numbers and it is expected that the interplay of all processes changes for high activity. First insights along this line predict a $t^{-1/4}$ scaling of the survival probability of highly persistent agents in the non-resetting case and for particles initially aligned parallel to the wall, highlighting the distinct physics that can arise in this limit.[53] For instance, an agent departing away from the wall and swimming persistently at high Péclet number is unlikely to reach the wall and it would be interesting to see what the resetting mechanism changes in this case. While we have here integrated out the direction parallel to the wall, it would be interesting to explore where the particles hit the wall.

While we have considered the effect of simultaneous resetting of both the position and orientation, the behavior of only resetting the position or the orientation is important for identifying optimal resetting protocols in active systems. The process of resetting the particle's position while orientation diffuses depends on the relative importance of the resetting rate and the rotational diffusivity, Λ. Thus, in the regime of large rotational diffusivity $\Lambda \lesssim 1$, this problem is expected to reduce to the situation, whereby the angle after each reset is chosen randomly. In the regime of low rotational diffusivity $\Lambda \gtrsim 1$, the initial orientation is expected to play a crucial role that needs to be further elucidated. Resetting of the orientation[54] towards the wall will decrease the FPT, yet in this context considering the associated cost may be important.

Since the agent considered here is active, there are even more directions in which one can extend this work. Experimental realizations of positional stochastic resetting for passive particles have been achieved through different implementations[55,56] and have yielded validation of the underlying theory. This is particularly relevant for our case, where the question of resetting a microscale active agent is experimentally not straightforward.[57] Resetting is naturally associated with a thermodynamic cost[58–62] and as these active agents are generally immersed in a fluidic environment they would also need to overcome an additional

drag force and withstand shear-induced reorientations, not present in passive systems.[63] Further experimental efforts may focus on designing efficient resetting protocols for microswimmers, guided by our theoretical predictions.

In the context of foraging and other target-search problems, stochastic resetting is often depicted as an advantageous search strategy[56,64] but in a lot of situations agents are active and cannot be said to simply perform Brownian motion. One experimental example at the macroscale represents experiments on centimeter-sized, active robots, whose orientation is subject to resetting *via* light stimuli, providing potential insights into the optimal foraging and homing behaviors of animals.[65] Unraveling the interplay of orientational and positional resetting in complex environments, including quenched disorder, boundaries,[66,67] and external fields,[68,69] is important for identifying optimal strategies of biological systems to find targets without being trapped in the environment. Furthermore, focusing on different swimming strategies that go beyond the paradigmatic active Brownian particle model, such as chiral motion,[70] represents an exciting future research avenue.

Conflicts of interest

There are no conflicts to declare.

Data availability

Most data can be generated by using the formulas provided in the manuscript. The data that support the findings of this study are available upon reasonable request from the authors.

Appendices

The appendix contains a summary of the perturbative approach used to compute the propagator in the absence of resetting [Section A], the expression of the MFPT in the presence of resetting [Section B], a validation of the perturbative approach for intermediate Péclet numbers [Section C], and finally the details of our simulations [Section D].

A: Perturbative approach

In this section, we provide additional details regarding the approach we used for the FPT statistics of an ABP without stochastic resetting in ref. 52. Therefore, we insert the expansion in eqn (10) up to second order in the Péclet number into the Laplace transform of the Fokker–Planck equation [eqn (9)] to obtain a coupled set of equations that are solved iteratively:

$$(s-\mathcal{H}_0)\widehat{\mathbb{P}}_0^{\mathrm{o}} = \delta(Z-Z_0)\delta(\vartheta-\vartheta_0), \tag{A1a}$$

$$(s-\mathcal{H}_0)\widehat{\mathbb{P}}_1^{\mathrm{o}} = \mathcal{V}\widehat{\mathbb{P}}_0^{\mathrm{o}}, \tag{A1b}$$

$$(s-\mathcal{H}_0)\widehat{\mathbb{P}}_2^{\mathrm{o}} = \mathcal{V}\widehat{\mathbb{P}}_1^{\mathrm{o}}. \tag{A1c}$$

The contribution of order $i+1$ can be computed from the contribution of order i through:

$$\widehat{\mathbb{P}}_{i+1}^{\mathrm{o}}(Z,\vartheta,s|Z_0,\vartheta_0) = \int_0^\infty\int_0^{2\pi} G(s,Z,\vartheta,Z',\vartheta')\left[\mathcal{V}\widehat{\mathbb{P}}_i^{\mathrm{o}}\right](Z',\vartheta',s|Z_0,\vartheta_0)\mathrm{d}Z'\mathrm{d}\vartheta', \tag{A2}$$

where G denotes the Green's function solving eqn (A1a) with boundary condition $G(s,Z=0,\vartheta,Z',\vartheta')=0$. Computing G is done by first solving the equation for an unbounded domain (whose solution we denote by G^u) and subtracting the contribution of an image solution to impose the boundary condition:

$$\begin{aligned} G(s,Z,\vartheta,Z',\vartheta') &= G^u(s,Z,\vartheta,Z',\vartheta') - G^u(s,Z,\vartheta,-Z',\vartheta') \\ &= \frac{1}{2\pi}\sum_{\ell=-\infty}^{\infty} \mathrm{e}^{i\ell(\vartheta'-\vartheta)}\frac{1}{2p_\ell}\left(\mathrm{e}^{-p_\ell|Z-Z'|} - \mathrm{e}^{-p_\ell|Z+Z'|}\right), \end{aligned} \tag{A3}$$

where $p_\ell^2 = s+\gamma l^2$. We further note that due to the symmetry of the coefficients, $p_\ell = p_{-\ell}$, there is no need to change the angular part of the image solution.

Each contribution to the survival probability is then obtained by marginalizing over the position:

$$\hat{S}_i^{\mathrm{o}}(s|Z_0,\vartheta_0) = \int_0^\infty \widehat{\mathbb{P}}_i^{\mathrm{o}}(s,Z|Z_0,\vartheta_0)\mathrm{d}Z. \tag{A4}$$

The zeroth-order solution, corresponding to the survival probability of a passive particle, is

$$\hat{S}_0^{\mathrm{o}}(s|Z_0) = \frac{1}{s}\left(1-\mathrm{e}^{-\sqrt{s}Z_0}\right), \tag{A5}$$

and the first- and second-order corrections read:

$$\hat{S}_1^{\mathrm{o}}(s|Z_0,\vartheta_0) = \frac{\cos(\vartheta_0)}{\gamma\sqrt{s}}\left(\mathrm{e}^{-\sqrt{s}Z_0} - \mathrm{e}^{-\sqrt{s+\gamma}Z_0}\right), \tag{A6}$$

$$\begin{aligned} \hat{S}_2^{\mathrm{o}}(s,|Z_0,\vartheta_0) &= \\ &-\frac{\mathrm{e}^{-Z_0\left(\sqrt{s}+\sqrt{s+\gamma}+\sqrt{s+4\gamma}\right)}}{24\sqrt{s}\sqrt{s+\gamma}\gamma^2}\Big[6\mathrm{e}^{Z_0\sqrt{s+4\gamma}} \\ &\times\left(2\mathrm{e}^{\sqrt{s}Z_0}(s+\gamma)+\mathrm{e}^{Z_0\sqrt{s+\gamma}}(-2s-2\gamma+Z_0\gamma\sqrt{s+\gamma})\right) \\ &+\left(3\mathrm{e}^{Z_0\left(\sqrt{s+\gamma}+\sqrt{s+4\gamma}\right)}\sqrt{s}\sqrt{s+\gamma} - 4\mathrm{e}^{Z_0\left(\sqrt{s}+\sqrt{s+4\gamma}\right)}(s+\gamma)\right. \\ &\left.+\mathrm{e}^{Z_0(\sqrt{s}+\sqrt{s+\gamma})}\left(4s+4\gamma-3\sqrt{s}\sqrt{s+\gamma}\right)\right)\cos(2\vartheta_0)\Big]. \end{aligned} \tag{A7}$$

Finally, the survival probability in Laplace space in the absence of resetting up to second order in the Péclet number is given by $\hat{S}^{\mathrm{o}} = \hat{S}_0^{\mathrm{o}} + \mathrm{Pe}\,\hat{S}_1^{\mathrm{o}} + \mathrm{Pe}^2\,\hat{S}_2^{\mathrm{o}}$. The latter is inserted into eqn (5) in the main text to obtain the survival probability with resetting.

B: Analytical expression for the MFPT

The analytical expression of the MFPT of the ABP up to second order in the Péclet number in Laplace space reads

$$\mathbb{E}[F_T](Z_0,\vartheta_0) = \frac{f(Z_0,\vartheta_0)}{g(Z_0,\vartheta_0)}, \tag{B1}$$

where

$$\begin{aligned} f(Z_0,\vartheta_0) &= 24\gamma^2 - 12e^{-Z_0\sqrt{\Lambda+\gamma}}\mathrm{Pe}^2\sqrt{\Lambda(\Lambda+\gamma)} \\ &+ \frac{1}{\sqrt{\Lambda+\gamma}}\Big[6e^{-\sqrt{\Lambda}Z_0}\Big(-4\gamma^2\sqrt{\Lambda+\gamma} \\ &+ \mathrm{Pe}^2\Big(2\sqrt{\Lambda}(\Lambda+\gamma) - Z_0\gamma\sqrt{\Lambda(\Lambda+\gamma)}\Big)\Big)\Big] \\ &+ 24\Big(e^{-\sqrt{\Lambda}Z_0} - e^{-\sqrt{\Lambda+\gamma}Z_0}\Big)\mathrm{Pe}\sqrt{\Lambda}\gamma\cos(\vartheta_0) \\ &+ \mathrm{Pe}^2\cos(2\vartheta_0)\Big(-3e^{-\sqrt{\Lambda}Z_0}\Lambda \\ &+ 4e^{-Z_0\sqrt{\Lambda+\gamma}}\sqrt{\Lambda(\Lambda+\gamma)} \\ &+ e^{-Z_0\sqrt{\Lambda+4\gamma}}\Big(3\Lambda - 4\sqrt{\Lambda(\Lambda+\gamma)}\Big)\Big), \end{aligned} \tag{B2a}$$

$$\begin{aligned} g(Z_0,\vartheta_0) &= \Lambda\Big(6\Big(2e^{-Z_0\sqrt{\Lambda+\gamma}}\mathrm{Pe}^2\sqrt{\Lambda(\Lambda+\gamma)} \\ &+ e^{-\sqrt{\Lambda}Z_0}\Big(4\gamma^2 + \mathrm{Pe}^2\Big(\sqrt{\Lambda}Z_0\gamma - 2\sqrt{\Lambda(\Lambda+\gamma)}\Big)\Big)\Big) \\ &+ 24\Big(e^{-Z_0\sqrt{\gamma+\Lambda}} - e^{-\sqrt{\Lambda}Z_0}\Big)\mathrm{Pe}\sqrt{\Lambda}\gamma\cos(\vartheta_0) \\ &+ \mathrm{Pe}^2\cos(2\vartheta_0)\Big(3e^{-\sqrt{\Lambda}Z_0}\Lambda \\ &- 4e^{-Z_0\sqrt{\Lambda+\gamma}}\sqrt{\Lambda(\Lambda+\gamma)} \\ &+ e^{-Z_0\sqrt{\Lambda+4\gamma}}\Big(4\sqrt{\Lambda(\Lambda+\gamma)} - 3\Lambda\Big)\Big)\Big). \end{aligned} \tag{B2b}$$

Expansion of the full expression up to second order in the Péclet number results in

$$\mathbb{E}[F_T] = \mathbb{E}_0[F_T] + \mathrm{Pe}\,\mathbb{E}_1[F_T] + \mathrm{Pe}^2\,\mathbb{E}_2[F_T] + \mathcal{O}(\mathrm{Pe}^3) \tag{B3}$$

with $\mathbb{E}_0[F_T] = \mathbb{E}[F_T]_B$ [eqn (16)] and the activity-induced contributions:

$$\mathbb{E}_1[F_T] = \frac{e^{Z_0\sqrt{\Lambda}}}{\gamma\sqrt{\Lambda}}\Big(e^{Z_0\left(\sqrt{\Lambda}-\sqrt{\gamma+\Lambda}\right)} - 1\Big)\cos(\vartheta_0), \tag{B4a}$$

$$\begin{aligned} \mathbb{E}_2[F_T] = \frac{e^{-Z_0\left(3\sqrt{\gamma+\Lambda}+\sqrt{4\gamma+\Lambda}\right)}}{24\gamma^2\sqrt{\Lambda(\Lambda+\gamma)}}\Big[&-6e^{Z_0\left(\sqrt{\Lambda}+2\sqrt{\gamma+\Lambda}+\sqrt{4\gamma+\Lambda}\right)} \\ &\times\Big(2e^{Z_0\sqrt{\Lambda}}(\gamma+\Lambda) + e^{Z_0\sqrt{\gamma+\Lambda}} \\ &\times\Big(-2\Lambda+\gamma\Big(-2+Z_0\sqrt{\gamma+\Lambda}\Big)\Big)\Big) \\ &+ 24e^{Z_0\left(\sqrt{\Lambda}+\sqrt{\gamma+\Lambda}+\sqrt{4\gamma+\Lambda}\right)}\Big(e^{Z_0\sqrt{\Lambda}} - e^{Z_0\sqrt{\gamma+\Lambda}}\Big)^2\cos(\vartheta_0)^2 \\ &+ e^{Z_0\left(\sqrt{\Lambda}+2\sqrt{\gamma+\Lambda}\right)}\Big(4e^{Z_0\left(\sqrt{\Lambda}+\sqrt{4\gamma+\Lambda}\right)}(\gamma+\Lambda) \\ &- 3e^{Z_0\left(\sqrt{\gamma+\Lambda}+\sqrt{4\gamma+\Lambda}\right)}\sqrt{\Lambda(\gamma+\Lambda)} \\ &+ e^{Z_0\left(\sqrt{\Lambda}+\sqrt{\gamma+\Lambda}\right)}\Big(3\sqrt{\Lambda(\gamma+\Lambda)} - 4\gamma - 4\Lambda\Big)\Big)\cos(2\vartheta_0)\Big]. \end{aligned} \tag{B4b}$$

C: Validation of the perturbation approach

In ref. 52, we show how the contributions of the first- and second-order corrections affect the FPT statistics for a non-resetting particle, and give a recursive scheme to compute higher-order corrections. In particular, the second-order term captures the essential orientational degrees of freedom; higher-order corrections typically contribute negligibly to the statistics. This is why all our results are obtained by truncating the series expansion of $\hat{S}^o$ at the second-order in Pe. To check the range of validity of our perturbation approach for the computation of the MFPT, we also plot $\mathbb{E}[F_t]$ as a function of the Péclet number, Pe (*i.e.*, our perturbation parameter). Our results shown in Fig. 9 indicate that, at least until a resetting rate $\Lambda = 3$, the theory provides good agreement with simulations up to $\mathrm{Pe} \approx 1$. It also remains valid up to $\mathrm{Pe} = 3$ for the largest resetting rate $\Lambda = 3$, whereas discrepancies start to emerge as the resetting rate is lowered. This can be explained by considering that for $\Lambda = 3$, the length traveled by the particle before resetting is

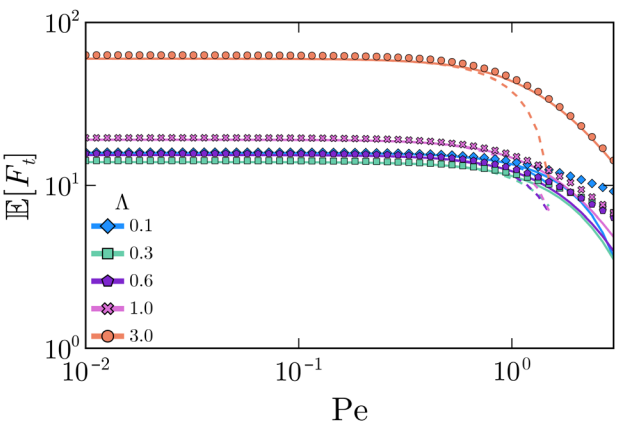

Fig. 9 MFPT $\mathbb{E}[F_t]$ as a function of the Péclet number Pe for several resetting rates Λ. Here, the initial distance is $z_0/a = 3$ and the initial orientation ϑ_0 is chosen randomly. Solid lines and symbols denote theory and simulations, respectively. Dashed lines correspond to the result given by eqn (B3).

smaller than the persistence length $l_R/l_p = \gamma/(\Lambda + \gamma) \ll 1$. Thus, the agent essentially reaches the wall without fully taking advantage of persistent motion. For lower resetting rates the effects of active motion can fully develop, leading to the observed discrepancies between theory and simulations.

In the same figure, we also plot as dashed lines the expansion of the MFPT given by eqn (B3) and see that it performs worse at larger Pe. Even though the expression given by eqn (B1) is exact up to second order in the Péclet number, it is a ratio and thus contains terms of mixed-order. Computing its series around zero naturally leads to truncating higher-order terms to approximate $\mathbb{E}[F_T]$. Our results show that the agreement with numerics becomes considerably worse at Pe $\gtrsim$ 1, which is why we use eqn (B1) throughout the manuscript.

D: Computer simulations

To perform stochastic simulations, we discretize eqn (1a) and (1b) according to the Euler–Maruyama scheme:

$$\boldsymbol{r}(t+\Delta t) = \boldsymbol{r}(t) + v\boldsymbol{e}(\vartheta(t))\Delta t + \sqrt{2D\Delta t}\boldsymbol{N}_t(0,1), \quad \text{(D1a)}$$

$$\vartheta(t+\Delta t) = \vartheta(t) + \sqrt{2D_{\mathrm{rot}}\Delta t}N_{\mathrm{r}}(0,1), \quad \text{(D1b)}$$

where $\Delta t = 10^{-3}\tau$ is the time-step, $\boldsymbol{N}_t(0,1)$ and $N_r(0,1)$ are independent, normally-distributed random variable with zero mean and unit variance. Furthermore, the statistics are obtained by simulating trajectories for 10^5 particles.

Acknowledgements

We gratefully acknowledge discussions with Thomas Franosch and Magali Le Goff. Open Access funding provided by the Max Planck Society.

References

1 M. R. Evans and S. N. Majumdar, Diffusion with Stochastic Resetting, *Phys. Rev. Lett.*, 2011, **106**(16), 160601.
2 J. Whitehouse, M. R. Evans and S. N. Majumdar, Effect of Partial Absorption on Diffusion with Resetting, *Phys. Rev. E: Stat., Nonlinear, Soft Matter Phys.*, 2013, **87**(2), 022118.
3 L. Kusmierz, S. N. Majumdar, S. Sabhapandit and G. Schehr, First Order Transition for the Optimal Search Time of Lévy Flights with Resetting, *Phys. Rev. Lett.*, 2014, **113**(22), 220602.
4 L. Kuśmierz and E. Gudowska-Nowak, Optimal First-Arrival Times in Lévy Flights with Resetting, *Phys. Rev. E: Stat., Nonlinear, Soft Matter Phys.*, 2015, **92**(5), 052127.
5 M. Radice and G. Cristadoro, Optimizing Leapover Lengths of Lévy Flights with Resetting, *Phys. Rev. E*, 2024, **110**(2), L022103.
6 S. Eule and J. J. Metzger, Non-Equilibrium Steady States of Stochastic Processes with Intermittent Resetting, *New J. Phys.*, 2016, **18**(3), 033006.
7 V. P. Shkilev, Continuous-Time Random Walk under Time-Dependent Resetting, *Phys. Rev. E*, 2017, **96**(1), 012126.
8 C. Kurzthaler, Y. Zhao, N. Zhou, J. Schwarz-Linek, C. Devailly and J. Arlt, *et al.*, Characterization and Control of theRun-and-Tumble Dynamics of *Escherichia coli*, *Phys. Rev. Lett.*, 2024, **132**(3), 038302.
9 Y. Zhao, C. Kurzthaler, N. Zhou, J. Schwarz-Linek, C. Devailly and J. Arlt, *et al.*, Quantitative Characterization of Run-and-Tumble Statistics in Bulk Bacterial Suspensions, *Phys. Rev. E*, 2024, **109**(1), 014612.
10 O. Tal-Friedman, Y. Roichman and S. Reuveni, Diffusion with Partial Resetting, *Phys. Rev. E*, 2022, **106**(5), 054116.
11 M. Biroli, Y. Feld, A. K. Hartmann, S. N. Majumdar and G. Schehr, Resetting by Rescaling: Exact Results for a Diffusing Particle in One Dimension, *Phys. Rev. E*, 2024, **110**(4), 044142.
12 A. Pal, A. Kundu and M. R. Evans, Diffusion under Time-Dependent Resetting, *J. Phys. A: Math. Theor.*, 2016, **49**(22), 225001.
13 V. Méndez, R. Flaquer-Galmés and D. Campos, First-Passage Time of a Brownian Searcher with Stochastic Resetting to Random Positions, *Phys. Rev. E*, 2024, **109**(4), 044134.
14 M. Luby, A. Sinclair and D. Zuckerman, Optimal Speedup of Las Vegas Algorithms, *Inf. Process. Lett.*, 1993, **47**(4), 173–180.
15 A. Montanari and R. Zecchina, Optimizing Searches *via* Rare Events, *Phys. Rev. Lett.*, 2002, **88**(17), 178701.
16 O. Blumer, S. Reuveni and B. Hirshberg, Stochastic Resetting for Enhanced Sampling, *J. Phys. Chem. Lett.*, 2022, **13**(48), 11230–11236.
17 O. Blumer, S. Reuveni and B. Hirshberg, Combining Stochastic Resetting with Metadynamics to Speed-up Molecular Dynamics Simulations, *Nat. Commun.*, 2024, **15**(1), 240.
18 M. Coppey, O. Bénichou, R. Voituriez and M. Moreau, Kinetics of Target Site Localization of a Protein on DNA: A Stochastic Approach, *Biophys. J.*, 2004, **87**(3), 1640–1649.
19 J. Chmeliov, L. Valkunas, T. P. J. Krüger, C. Ilioaia and R. van Grondelle, Fluorescence Blinking of Single Major Light-Harvesting Complexes, *New J. Phys.*, 2013, **15**(8), 085007.
20 S. Ghosh, B. Mishra, A. B. Kolomeisky and D. Chowdhury, First-Passage Processes on a Filamentous Track in a Dense Traffic: Optimizing Diffusive Search for a Target in Crowding Conditions, *J. Stat. Mech.: Theory Exp.*, 2018, **2018**(12), 123209.
21 O. Bénichou, M. Coppey, M. Moreau, P. H. Suet and R. Voituriez, Optimal Search Strategies for Hidden Targets, *Phys. Rev. Lett.*, 2005, **94**(19), 198101.
22 O. Bénichou, C. Loverdo, M. Moreau and R. Voituriez, Intermittent Search Strategies, *Rev. Mod. Phys.*, 2011, **83**(1), 81–129.
23 S. S. Suarez and A. A. Pacey, Sperm Transport in the Female Reproductive Tract, *Hum. Reprod. Update*, 2006, **12**(1), 23–37.
24 E. Lauga and T. R. Powers, The Hydrodynamics of Swimming Microorganisms, *Rep. Prog. Phys.*, 2009, **72**(9), 096601.
25 *The Physics of Foraging: An Introduction to Random Searches and Biological Encounters*, ed. G. M. Viswanathan, Cambridge University Press, Cambridge, New York, 2011.
26 C. Bechinger, R. Di Leonardo, H. Löwen, C. Reichhardt, G. Volpe and G. Volpe, Active Particles in Complex and Crowded Environments, *Rev. Mod. Phys.*, 2016, **88**(4), 045006.
27 E. Lauga, The Fluid Dynamics of Cell Motility, *Cambridge Texts in Applied Mathematics*, Cambridge University Press, Cambridge, 2020.

28 *Out-of-Equilibrium Soft Matter*, ed. C. Kurzthaler, L. Gentile and H. A. Stone, The Royal Society of Chemistry, 1st edn, 2023.
29 *Target Search Problems*, ed. D. Grebenkov, R. Metzler and G. Oshanin, Springer Nature Switzerland, Cham, 1st edn, 2024.
30 S. J. Ebbens and J. R. Howse, In Pursuit of Propulsion at the Nanoscale, *Soft Matter*, 2010, **6**(4), 726–738.
31 L. Baraban, M. Tasinkevych, M. N. Popescu, S. Sanchez, S. Dietrich and O. G. Schmidt, Transport of Cargo by Catalytic Janus Micro-Motors, *Soft Matter*, 2011, **8**(1), 48–52.
32 W. Gao, A. Uygun and J. Wang, Hydrogen-Bubble-Propelled Zinc-Based Microrockets in Strongly Acidic Media, *J. Am. Chem. Soc.*, 2012, **134**(2), 897–900.
33 S. J. Ebbens, Active Colloids: Progress and Challenges towards Realising Autonomous Applications, *Curr. Opin. Colloid Interface Sci.*, 2016, **21**, 14–23.
34 T. Robin, S. Reuveni and M. Urbakh, Single-Molecule Theory of Enzymatic Inhibition, *Nat. Commun.*, 2018, **9**(1), 779.
35 A. Aziz, D. Karnaushenko, N. Koukourakis, J. W. Czarske, O. G. Schmidt and M. Medina-Sánchez, *Tracking of Magnetic Micromotors in Confined Channels Through Scattering Tissue*. In: 2021 IEEE 15th International Conference on Nano/Molecular Medicine & Engineering (NANOMED), 2021, pp. 57–62.
36 A. Aziz, R. Nauber, A. S. Iglesias, L. M. Liz-Marzán, O. G. Schmidt and M. Medina-Sánchez, *Imaging and Control of Nanomaterial-Decorated Micromotors*. In: 2022 International Conference on Manipulation, Automation and Robotics at Small Scales (MARSS), 2022, pp. 1–6.
37 R. Nauber, S. R. Goudu, M. Goeckenjan, M. Bornhäuser, C. Ribeiro and M. Medina-Sánchez, Medical Microrobots in Reproductive Medicine from the Bench to the Clinic, *Nat. Commun.*, 2023, **14**(1), 728.
38 L. Angelani, R. Di Leonardo and M. Paoluzzi, First-Passage Time of Run-and-Tumble Particles, *Eur. Phys. J. E: Soft Matter Biol. Phys.*, 2014, **37**(7), 59.
39 K. Malakar, V. Jemseena, A. Kundu, K. Vijay Kumar, S. Sabhapandit and S. N. Majumdar, *et al.*, Steady State, Relaxation and First-Passage Properties of a Run-and-Tumble Particle in One- Dimension, *J. Stat. Mech.: Theory Exp.*, 2018, **2018**(4), 043215.
40 G. Tucci, A. Gambassi, S. N. Majumdar and G. Schehr, First-Passage Time of Run-and-Tumble Particles with Noninstantaneous Resetting, *Phys. Rev. E*, 2022, **106**(4), 044127.
41 D. Vinod, A. G. Cherstvy, W. Wang, R. Metzler and I. M. Sokolov, Nonergodicity of Reset Geometric Brownian Motion, *Phys. Rev. E*, 2022, **105**(1), L012106.
42 F. Di Trapani, T. Franosch and M. Caraglio, Active Brownian Particles in a Circular Disk with an Absorbing Boundary, *Phys. Rev. E*, 2023, **107**(6), 064123.
43 M. Guéneau, S. N. Majumdar and G. Schehr, Optimal Mean First-Passage Time of a Run-and-Tumble Particle in a Class of One-Dimensional Confining Potentials, *Europhys. Lett.*, 2024, **145**(6), 61002.
44 M. Guéneau, S. N. Majumdar and G. Schehr, Run-and-Tumble Particle in One-Dimensional Potentials: Mean First-Passage Time and Applications, *Phys. Rev. E*, 2025, **111**(1), 014144.
45 J. R. Howse, R. A. L. Jones, A. J. Ryan, T. Gough, R. Vafabakhsh and R. Golestanian, Self-Motile Colloidal Particles: From Directed Propulsion to Random Walk, *Phys. Rev. Lett.*, 2007, **99**(4), 048102.
46 P. Romanczuk, M. Bär, W. Ebeling, B. Lindner and L. Schimansky-Geier, Active Brownian Particles, *Eur. Phys. J.: Spec. Top.*, 2012, **202**(1), 1–162.
47 B. ten Hagen, S. van Teeffelen and H. Löwen, Brownian Motion of a Self-Propelled Particle, *J. Phys.: Condens. Matter*, 2011, **23**(19), 194119.
48 C. Kurzthaler, S. Leitmann and T. Franosch, Intermediate Scattering Function of an Anisotropic Active Brownian Particle, *Sci. Rep.*, 2016, **6**(1), 36702.
49 C. Kurzthaler, C. Devailly, J. Arlt, T. Franosch, W. C. K. Poon and V. A. Martinez, *et al.*, Probing the Spatiotemporal Dynamics of Catalytic Janus Particles with Single-Particle Tracking and Differential Dynamic Microscopy, *Phys. Rev. Lett.*, 2018, **121**(7), 078001.
50 J. Masoliver, Telegraphic Processes with Stochastic Resetting, *Phys. Rev. E: Stat., Nonlinear, Soft Matter Phys.*, 2019, **99**(1), 012121.
51 M. R. Evans, S. N. Majumdar and G. Schehr, Stochastic Resetting and Applications, *J. Phys. A: Math. Theor.*, 2020, **53**(19), 193001.
52 Y. Baouche, M. Le Goff, C. Kurzthaler and T. Franosch, First-Passage-Time Statistics of Active Brownian Particles: A Perturbative Approach, *Phys. Rev. E*, 2025, **111**(5), 054113.
53 U. Basu, S. N. Majumdar, A. Rosso and G. Schehr, Active Brownian Motion in Two Dimensions, *Phys. Rev. E*, 2018, **98**(6), 062121.
54 Y. Baouche, T. Franosch, M. Meiners and C. Kurzthaler, Active Brownian Particle under Stochastic Orientational Resetting, *New J. Phys.*, 2024, **26**(7), 073041.
55 O. Tal-Friedman, A. Pal, A. Sekhon, S. Reuveni and Y. Roichman, Experimental Realization of Diffusion with Stochastic Resetting, *J. Phys. Chem. Lett.*, 2020, **11**(17), 7350–7355.
56 S. Gupta and A. M. Jayannavar, Stochastic Resetting: A (Very) Brief Review, *Front. Phys.*, 2022, **10**, 789097.
57 I. Abdoli and A. Sharma, Stochastic Resetting of Active Brownian Particles with Lorentz Force, *Soft Matter*, 2021, **17**(5), 1307–1316.
58 J. Fuchs, S. Goldt and U. Seifert, Stochastic Thermodynamics of Resetting, *Europhys. Lett.*, 2016, **113**(6), 60009.
59 D. M. Busiello, D. Gupta and A. Maritan, Entropy Production in Systems with Unidirectional Transitions, *Phys. Rev. Res.*, 2020, **2**(2), 023011.
60 P. S. Pal, A. Pal, H. Park and J. S. Lee, Thermodynamic Trade-off Relation for First Passage Time in Resetting Processes, *Phys. Rev. E*, 2023, **108**(4), 044117.
61 J. C. Sunil, R. A. Blythe, M. R. Evans and S. N. Majumdar, The Cost of Stochastic Resetting, *J. Phys. A: Math. Theor.*, 2023, **56**(39), 395001.
62 J. Q. Toledo-Marín and D. Boyer, First Passage Time and Information of a One-Dimensional Brownian Particle with

Stochastic Resetting to Random Positions, *Phys. A*, 2023, **625**, 129027.

63 I. Abdoli, K. S. Olsen and H. Löwen, Shear-Driven Diffusion with Stochastic Resetting, *Phys. Fluids*, 2024, **36**(11), 117151.

64 P. C. Bressloff, Search Processes with Stochastic Resetting and Multiple Targets, *Phys. Rev. E*, 2020, **102**(2), 022115.

65 S. Paramanick, A. Biswas, H. Soni, A. Pal and N. Kumar, Uncovering Universal Characteristics of Homing Paths Using Foraging Robots, *PRX Life*, 2024, **2**(3), 033007.

66 E. Q. Z. Moen, K. S. Olsen, J. Rønning and L. Angheluta, Trapping of Active Brownian and Run-and-Tumble Particles: A First-Passage Time Approach, *Phys. Rev. Res.*, 2022, **4**(4), 043012.

67 G. Kumar Sar, A. Ray, D. Ghosh, C. Hens and A. Pal, Resetting-Mediated Navigation of an Active Brownian Searcher in a Homogeneous Topography, *Soft Matter*, 2023, **19**(24), 4502–4518.

68 B. Walter, G. Pruessner and G. Salbreux, First Passage Time Distribution of Active Thermal Particles in Potentials, *Phys. Rev. Res.*, 2021, **3**(1), 013075.

69 I. Abdoli, H. D. Vuijk, R. Wittmann, J. U. Sommer, J. M. Brader and A. Sharma, Stationary State in Brownian Systems with Lorentz Force, *Phys. Rev. Res.*, 2020, **2**(2), 023381.

70 K. S. Olsen and H. Löwen, Optimal Diffusion of Chiral Active Particles with Strategic Reorientations, *Phys. Rev. E*, 2024, **110**(6), 064606.